EFDA–JET–CP(12)02/01

P. Jacquet, F. Marcotte, L. Colas, G. Arnoux, V. Bobkov, Y. Corre, S. Devaux,
J-L Gardarein, E. Gauthier, M. Graham, E. Lerche, M-L. Mayoral,
I. Monakhov, F. Rimini, A. Sirinelli, D. Van Eester
and JET EFDA contributors

Characterisation of Local ICRF Heat Loads on the JET ILW

Characterisation of Local ICRF Heat Loads on the JET ILW

P. Jacquet[1], F. Marcotte[2], L. Colas[3], G. Arnoux[1], V. Bobkov[4], Y. Corre[3], S. Devaux[4], J-L Gardarein[5], E. Gauthier[3], M. Graham[1], E. Lerche[6], M-L. Mayoral[1], I. Monakhov[1], F. Rimini[1], A. Sirinelli[1], D. Van Eester[6] and JET EFDA contributors*

JET-EFDA, Culham Science Centre, OX14 3DB, Abingdon, UK

[1]EURATOM-CCFE Fusion Association, Culham Science Centre, OX14 3DB, Abingdon, OXON, UK
[2]Ecole Nationale des Ponts et Chaussées, F77455 Marne-la-Vallée, France
[3]CEA, IRFM, F-13108 Saint-Paul-Lez-Durance, France
[4]Max-Planck-Institut für Plasmaphysik, EURATOM-Assoziation, Garching, Germany
[5]Aix-Marseille University, IUSTI UMR 6995, 13013 Marseille, France
[6]Association EURATOM-Belgian State, ERM-KMS, Brussels, Belgium
** See annex of F. Romanelli et al, "Overview of JET Results", (23rd IAEA Fusion Energy Conference, Daejon, Republic of Korea (2010)).*

Preprint of Paper to be submitted for publication in Proceedings of the 20th International Conference on Plasma Surface Interactions , Eurogress, Aachen, Germany 21st May 2012 - 25th May 2012

ABSTRACT

When using ICRF, enhanced heat-fluxes are likely to develop on some plasma facing components close to the antennas. Experiments have recently been carried out on JET with the new ITER-Like-Wall (ILW) to characterise this phenomenon. Using Infra-Red thermography and thermal models of the tiles, heat-fluxes were evaluated from the surface temperature increase during the RF phase of L-mode plasmas. The maximum observed heat-flux intensity was ~ 4.5MW/m^2 when operating with $-\pi/2$ current drive strap phasing at power level of 2MW per antenna and with a 4cm distance between the plasma and the outer limiters. Heat-fluxes are reduced when using dipole strap phasing. The fraction of ICRF power directly dissipated on the antenna limiters or septa was in the range 2–10% for dipole phasing and 10–20% with $-\pi/2$ phasing.

1. INTRODUCTION

During the application of Ion Cyclotron Range of Frequency (ICRF) heating in Tore-Supra [1] and JET [2], local heat deposition in the vicinity of the antennas is observed. This phenomenon is attributed to the interaction of ICRF waves with the SOL plasma through RF sheath rectification [3]. Infra-red (IR) thermography was used with the JET carbon (C) wall to quantify heat-fluxes on the protection septa of the JET A2 antennas [2]. Surface temperature increases (~ 600 ^{o}C in some cases) were explained by large temperature gradients that developed in layers, poorly attached thermally to the tiles bulk, while these Plasma Facing Components (PFCs) were submitted to modest heat-fluxes (few MW/m^2). Since 2011, JET has operated with a new ITER-like wall consisting mainly of beryllium (Be) tiles in the chamber and tungsten tiles in the divertor [4]. Experiments were carried out recently to further characterize local ICRF heat deposition in JET with the following goals:

a) Analyse IR thermography data in the JET Be wall environment in order to quantify the heat-fluxes on the tiles surrounding the antennas.
b) Verify that these heat-fluxes do not exceed the thermal handling capabilities of the PFCs, and in particular make sure that the tiles are not at risk of melting.
c) Characterise spatial pattern and intensity parametric dependence of hot-spots in order to better understand RF sheath rectification, the long term goal being the optimisation of ICRF antenna designs [5] to minimize this effect which has detrimental consequences on local power dissipation and on impurity generation [6].
d) Provide experimental data that could be used for extrapolation to the ITER ICRF system.

2. JET A2 ANTENNA SYSTEM AND WIDE ANGLE IR CAMERA

Figure 1 shows a schematic top view of the JET tokamak. The A2 ICRF antennas A, B, C, and D and the ITER-Like ICRF antenna (ILA, not used in 2011) are represented as well as the camera view which covers antenna A, the ILA antenna and half of antenna B. Each A2 antenna [7] is a phased array of 4 poloidal straps; controlling the phase between straps allows waves to be launched with different $k_{//}$ spectra. Usually π (dipole phasing) or +/– $\pi/2$ phasing (current drive phasings)

between adjacent straps are used. The plasma facing part of the antennas is covered by a Faraday screen consisting of tilted Be rods. Each antenna is surrounded by two poloidal limiters made of Beryllium tiles, and a vertical Be septum is fitted at the centre (between straps 2 and 3) of each antenna. In the experiments described here straps 1&2 of A2 antennas A and B were fed by the same RF amplifiers through a 3dB hybrid coupler system. Straps 3&4 of antenna A were fed by independent amplifiers, and straps 3&4 of antenna B were not used.

The JET wide angle IR camera is described in [8]. The IR camera wavelength measurement range is 3.97-4.01μm. The pixel size of the camera is approximately 1.5 cm at distances corresponding to the antenna A septum. For the pulses described here the camera time resolution was 20 ms (50 Hz acquisition rate) and the exposure time was 600 μs. A two point Non-Uniformity Correction (NUC) was applied to the response of each pixel. In order to measure the Be wall temperature, the camera was calibrated as follows:

- Thermocouples (Tc) imbedded in some of the inner or outer wall Be tiles viewed by the camera were taken as temperature references.
- The temperature of the wall was increased step by step in a series of inner/outer limiter plasma pulses (RF not used in the outer limiter plamas).
- The IR camera was calibrated against the Tc measurements. Calibration data were recorded at the beginning of each JET pulse, before any heating was applied to the wall in order to ensure the thermal equilibrium of the Be tiles instrumented with Tcs (time between pulses at least 20 minutes).

The Be surface temperature is deduced from the IR measurements assuming that *DL* the response of each pixel is linear function of surface spectral emission in the camera wavelength range of measurement:

$$DL = a + \frac{b}{b^{hc/(\lambda kt)} - 1} \tag{1}$$

where h is the Planck constant, c is the speed of light in vacuum, k is the Boltzmann constant, λ is the centre of the camera wavelength range and T is the temperature in Kelvin. The calibration curve used to deduce the Be surface temperature from the IR signal is shown in Figure 2; the parameters *a* and *b* (Equation 1) were obtained from a fit procedure to the calibration data and extrapolation was used for the highest temperatures. This calibration is coherent with the Be emissivity in this wavelength range (ε_{Be} ~0.18) as evaluated independently in [9]. The error bars on Figure 2 represent the uncertainties in surface temperature from the IR data; they are derived from the scatter in the calibration data.

3. EVALUATION OF HEAT-FLUXES FROM SURFACE TEMPERATURE MEASUREMENTS

A linear deconvolution procedure [10] was used to determine the heat-flux on the Be PFCs seen

by the camera from the time response of surface temperature. In this procedure, the tile thermal properties are taken into account through the surface temperature response to a Heaviside step excitation with a reference heat-flux. This is obtained from modelling. The tiles of the septa and of the poloidal limiters around the ICRF antennas were modelled using the ANSYS^{TM,1} finite element software and with a simplified 1D finite difference model [11]. An example for a septum tile is shown in Figure 3. The thermal response can slightly change depending on the size of the heated area, which was adjusted in the ANSYS simulations to match the size of the hot-spots on the IR camera view. The simplified 1D model and ANSYS thermal responses are close for analysis times of ~ 20 s or shorter; this correspondence is even better when modelling the outer poloidal limiters tiles because castellations at the surface of the tiles [12] (~12–13mm) prevent lateral heat diffusion. The 1D reference responses were used in the deconvolution procedure to calculate the heat-fluxes presented in this paper. Overall the error on heat-fluxes from the uncertainty on the tile thermal response is estimated to be +/– 5%.

Figure 4 shows an example of the heat-flux estimated on the antenna A septum when monitoring the temperature of the most intense hot-spot for Pulse No: 81719, one of the pulses from the series described in section 4. In this pulse ($B_T = 2.5$ T, Ip = 2 MA, 3cm plasma outer-limiter distance in the equatorial plane), the ICRF power was launched by antenna A and B (2 MW launched ICRF power in total); only straps 1&2 were used with a strap phasing of Φ_2-$\Phi_1 = -\pi/2$. In this case the hot-spot on the antenna A septum corresponds to a heat-flux of ~1.8 MW/m^2. The calculated heat-flux when the ICRF power was turned off (t>11s) is close to zero (and, in particular, it does not become negative) which is an indication of the quality of our thermal model. The heat-flux 'in-rush' observed during the 1st second of the ICRF pulse corresponds to a phase where the antenna matching elements were moving and the strap phases and feeding voltages were not yet stabilized. In particular, there was a strong voltage in-balance in the transmission lines during this phase. This illustrates the importance of antenna strap feeding conditions in the RF sheath rectification and local heat deposition phenomena [5].

4. CHARACTERISATION OF LOCAL ICRF HEAT-LOADS

An IR frame for Pulse No: 81719 is shown in Figure 5. Hot-spots developed on the energized antenna septa and on the neighbouring limiters. These hot-spots were not observed when using remote antennas with the same amount of RF power and so cannot be attributed to fast ions escaping from the plasma. The exact hot-spot pattern can change, depending on: the antenna feeding conditions (strap phasing, number of straps energized); the plasma configuration, in particular on the antenna–plasma distance (which affects antenna loading and thus RF electric field at the antenna aperture); and the magnetic configuration which affects the field line incidence on the PFCs. A series of pulses were used to quantify the RF hot-spot intensity as a function of ICRF system and plasma parameters. In this series, straps 1&2 or 1,2,3&4 of antenna A were used together with straps 1&2 of antenna B. The ICRF power launched from antenna A and B was varied in the range 0.5-3 MW (27 kV max

[1] *ANSYS™ , ANSYS Inc., Canonsburg, PA 15317, USA.*

voltage in the transmission lines) with dipole or -π/2 strap phasing. The plasma parameters were: B_T in the range 2.4-2.5T; $I_p = 2$MA; L-mode plasma; H minority ICRF heating (~2% H concentration); and plasma outer-limiter distance in the range 3-6cm. Figure 6 summarizes the main dependencies of the ICRF hot-spot intensity. The most intense heat-flux around antenna A (the location could change from pulse to pulse depending on plasma and ICRF system configurations) is plotted as a function of the triple product $n_{e.,lim} \times V^2 \times N_{strap}$, where $n_{e,lim}$ is the electron density in the SOL at a mid-plane radius of 3.87m (1 cm in front of the main outer poloidal limiters) as estimated from reflectometry measurements [13] (Figure 1 shows reflectometer location). During the experiment, $n_{e,lim}$ was changed by varying the outer radius of the plasma. V is the ICRF forward voltage in the transmission lines feeding the straps, averaged over the active straps of antenna A, and N_{strap} is the number of active straps in antenna A. The hot-spot intensity increases with: the electron density at the outer limiter position; the RF voltage in the transmission lines feeding the antenna; and the number of active straps. Note that Figure 6 enables a simple assessment of the maximum hot-spot intensity, which is useful for the purpose of machine protection but it does not necessarily integrate all parameters influencing RF sheaths; in particular, the strap feeding conditions and the coupling resistance are expected to influence the structure of the RF electric field at the antenna aperture. Work is on-going to further characterize the importance of these parameters in the ICRF heat-loads. This apparent $n_{e.,lim} \times V^2$ scaling is different from the one proposed in previous experiments with the JET C wall ($n_{e.,lim} \times V$ as described in [2][14]), which would be coherent with simple RF sheath rectification models [15]. The observed V^2 dependence might partially be caused by ICRF power driven local modifications of the density in front of the antennas. The hot-spot intensity increased when using $-\pi/2$ strap phasing instead of dipole; asymmetric antenna phasings are indeed expected to increase $E_{//}$, the component of the electric field parallel to the (static) magnetic field excited at the antenna aperture which drives RF sheath rectification and enhanced heat-loads [5]. For reference, C wall measurements on septum A have been added in Figure 6. The heat-fluxes estimated on the Be tiles (free of surface deposit) and on the C tiles (where thermal models had to include a surface layer with poor thermal conductivity [2]) are of the same order.

The fraction of ICRF power dissipated on neighbouring limiters for antennas A and B and the septa located in the IR camera view was also evaluated. During ICRF pulse, the heat-flux was evaluated on a regular grid covering these PFCs. The power dissipated on these objects, P_{dissip}, was then obtained by integrating the heat-flux over the surfaces. The fraction of ICRF power directly dissipated locally was calculated as:

$$\eta_{ICRF} = (P_{dissip} - P_{cond}) / P_{ICRF} \quad (2)$$

P_{cond}, the conducted plasma power falling on the same limiters was evaluated as:

$$P_{cond} = \kappa(P_{tot} - P_{rad}) \times e^{-d/\lambda_{pwr}} \quad (3)$$

where P_{tot} is the total (ohmic and auxiliary) plasma heating power, and P_{rad} is the power radiated in the plasma core, d is the distance between plasma and outer poloidal limiters in the equatorial plane and λ_{pwr} is the power decay length. The proportionality factor, κ, and λ_{pwr} (~3cm) were evaluated from heat-flux measurements on the same PFCs in a series of pulses in which antennas A and B were not used and where d was scanned. The fraction of ICRF power dissipated through heating of neighbouring PFCs ranges between 10% and 20 % for $-\pi/2$ strap phasing and between 2% and 10 % for dipole phasing. No clear dependence with P_{ICRF} or with plasma-outer limiters distance was seen.

CONCLUSIONS

Simple thermal models of Be tiles, validated with ANSYS, have enabled reliable evaluation of heat-fluxes and characterisation of local heat-loads in the vicinity of energized ICRF antennas. The highest ICRF heat-fluxes observed on JET with the ILW (~4.5MW/m^2 normal flux on PFCs) were obtained when launching 3MW (antenna A+B) with $-\pi/2$ phasing and a plasma poloidal-limiter distance of 4 cm. In practice, ICRF operation is not limited by this phenomena on JET because typical ICRF pulse duration is < 10s, and because dipole phasing is usually used. However, these heat-flux values deserve further attention, in particular when compared to the engineering design targets (5 MW/m^2) for the ITER ICRF antenna Faraday screen and neighbouring blanket modules. Work is on-going to understand the dependence of local RF heat deposition on antenna feeding conditions. Also IR thermography measurements will be compared to RF sheath rectification models taking into account the $E_{//}$ RF electric field distribution at the antenna aperture calculated with the TOPICA code [16] and the field line incidence on the PFC's surface.

ACKNOWLEDGEMENTS

This work, supported by the European Communities under the contract of Association between EURATOM and CCFE, was carried out within the framework of the European Fusion Development Agreement. The views and opinions expressed herein do not necessarily reflect those of the European Commission. This work was also part-funded by the RCUK Energy Programme under grant EP/I501045.

REFERENCES

[1]. C.E. Thomas Jr, *et al*., Journal of Nuclear Materials **220-222** p531 (1995)
[2]. P. Jacquet, *et al*., Nuclear Fusion **51** (2011) 103018 (16pp)
[3]. J. R. Myra, *et al*., Nuclear Fusion **46** (2006) S455–S468
[4]. G. F. Matthews, *et al*., Physica Scripta **T128** (2007) 137–143
[5]. V. Bobkov, *et al*., in RF Power in Plasmas, AIP Conf. Proc. **1187** , pp 221-224 (2009)
[6]. V. Bobkov, *et al*., these proceedings (contributed talk O3)
[7]. A. Kaye, *et al*., SOFE Conf. Proc., 16th IEEE/NPSS Symposium, Vol. 1 p736 (1995)

[8]. E. Gauthier, *et al*., Fusion Engineering and Design **83** 1335-1340 (2007)
[9]. S. Devaux, *et al*., these proceedings (contribution P3-086)
[10]. J.-L. Gardarein, *et al*., Fusion Engineering and Design **83** pp 759-765 (2008)
[11]. M. Necati Ozisik, Finite Difference Methods in Heat Transfer (CRC Press, Boca Raton, FL, 1994)
[12]. V. Riccardo, Journal of Nuclear Materials **390-391** (2009) 895–899
[13]. A. Sirinelli, et al., Review of Scientific Instruments **81**, 10D939 (2010)
[14]. L. Colas, *et al*., in RF Power in Plasmas, AIP Conf. Proc. 1187 , pp 133-136 (2009)
[15]. F. W. Perkins, *et al*., Nuclear Fusion **29** No.4 pp.583-592 (1989)
[16]. V. Lancellotti, *et al*., 2006 Nuclear Fusion **46** S476–99

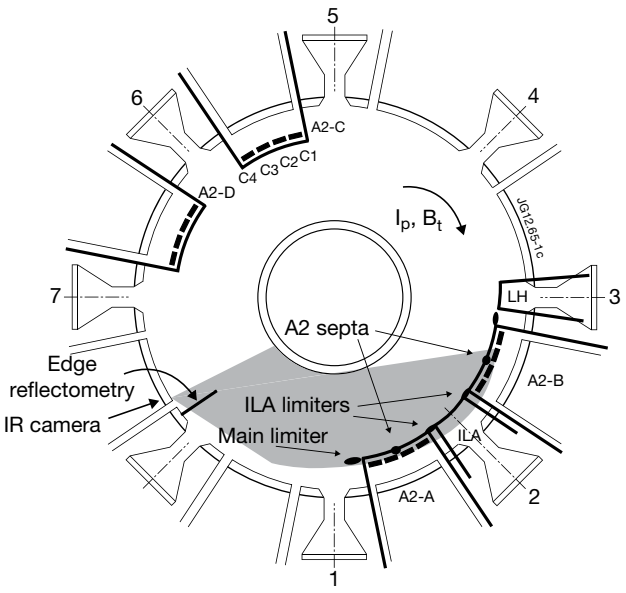

Figure 1: Top view of JET, showing the JET ICRF antennas (A, B, C, D, and ILA). The IR camera view is indicated in grey. The poloidal limiters and antenna septa seen by the camera are indicated with arrows. The line of sight of the edge reflectometer (close to the plasma midplane) is also shown.

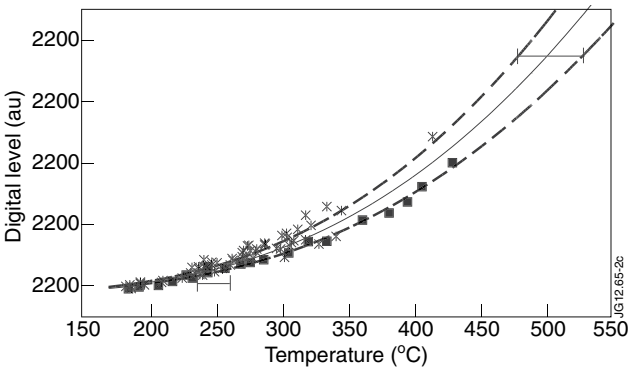

Figure 2: Wide angle IR camera calibration curve. Calibration data using thermocouple (Tc) measurements from the inner poloidal limiter (crosses) and the outer poloidal limiter (squares) are shown. The dotted lines are the calibration curve when using the inner poloidal Tcs only (top dotted line) or the outer Poloidal Tcs only (bottom dotted lines).

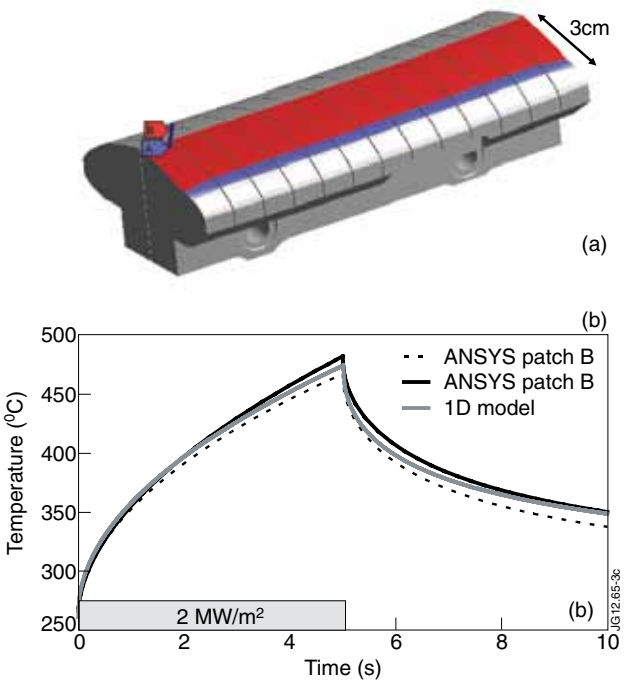

Figure 3: ICRF antenna septum tile thermal modelling. (a) ANSYS model of the tile. The surface temperature response at the centre of the heated area was computed when applying a 2MW/m^2/5s heat-flux on the tile surface, the heating patch width is 3cm (A) or 2.5cm (B). (b) Surface temperature response as modelled with ANSYS and a simplified 1D model.

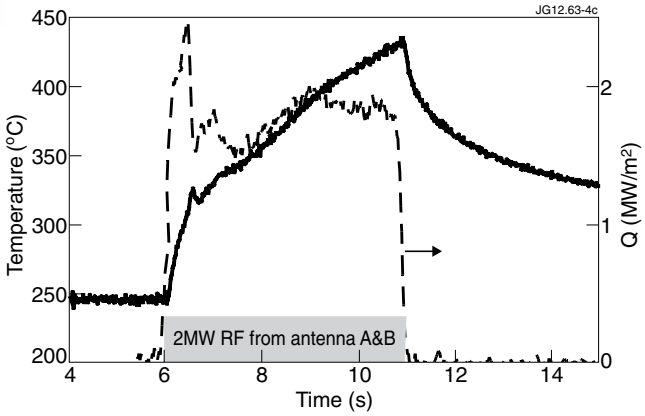

Figure 4: Evaluation of the heat-flux on antenna A septum during an ICRF pulse. The solid line is the surface temperature measured by the IR camera. The dotted line is the heat-flux evaluated on the surface.

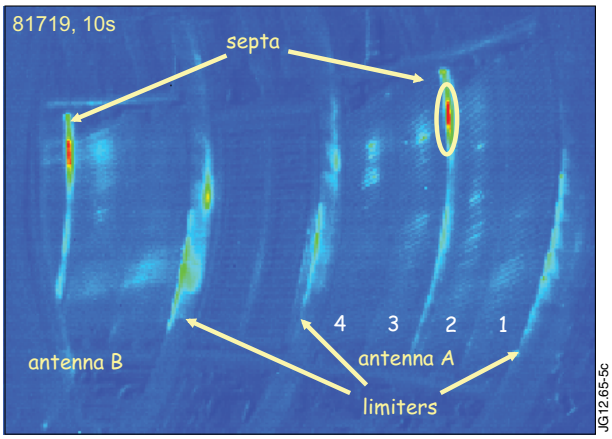

Figure 5: IR view of A and B antennas. In this pulse only straps 1,2 are energized. Hot-spots can be observed on the antenna septa, and on the poloidal limiters adjacent to the antennas. The area analysed in Figure 4 is encircled.

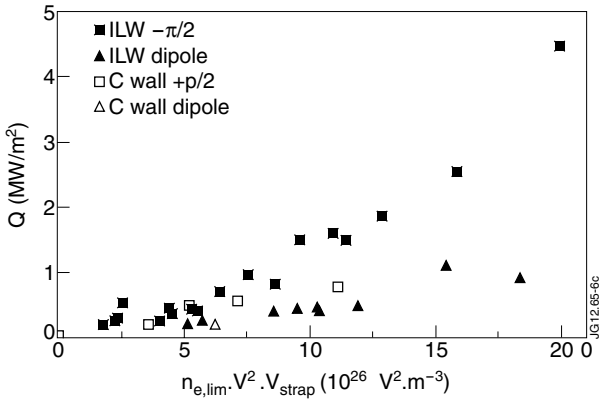

Figure 6: Maximum heat-flux measured around antenna A plotted vs $n_{e,lim} \times V^2 \times N_{strap}$. Squares are for –π/2 strap phasing, triangles are for dipole phasing. JET C wall measurements [2] are indicated with open symbols (47 MHz, +π/2-squares, or dipole-triangle).